Eur J Vasc Endovasc Surg (2019) 58, 746—755

Quantitative Stent Graft Motion in ECG Gated CT by Image Registration and Segmentation: In Vitro Validation and Preliminary Clinical Results

Maaike A. Koenrades [a,b,c,*], Esmeralda M. Struijs [d], Almar Klein [e], Hendrik Kuipers [c], Michel M.P.J. Reijnen [a,f], Cornelis H. Slump [c], Robert H. Geelkerken [a,b]

[a] Multi-modality Medical Imaging (M3I) group, Faculty of Science and Technology, Technical Medical Centre, University of Twente, Enschede, the Netherlands
[b] Department of Vascular Surgery, Medisch Spectrum Twente, Enschede, the Netherlands
[c] Robotics and Mechatronics (RaM) group, Faculty of Electrical Engineering, Mathematics and Computer Science, Technical Medical Centre, University of Twente, Enschede, the Netherlands
[d] Technical Medicine, Faculty of Science and Technology, Technical Medical Centre, University of Twente, Enschede, the Netherlands
[e] Independent Scholar, Enschede, the Netherlands
[f] Department of Vascular Surgery, Rijnstate, Arnhem, the Netherlands

WHAT THIS PAPER ADDS

The present article establishes a novel method to quantify and visualise stent graft motion in multiphasic ECG gated computed tomography using image registration techniques. In vitro validation demonstrated adequate accuracy for quantifying abdominal aortic stent graft displacement. The methodology was successfully applied to clinical data of patients treated by endovascular aneurysm repair (EVAR) with different stent graft designs. This novel methodology enables provision of accurate data characterising the in situ motions of stent grafts in the endovascular environment. This may have a major impact on stent graft design and early prediction of failure in post-market evaluations of new or modified devices.

Objectives: The dynamic endovascular environment of stent grafts may influence long term outcome after endovascular aneurysm repair (EVAR). The sealing and fixation of a stent graft to the aortic wall is challenged at every heartbeat, yet knowledge of the cardiac induced dynamics of stent grafts is sparse. Understanding the stent—artery interaction is crucial for device development and may aid the prediction of failure in the individual patient. The aim of this work was to establish quantitative stent graft motion in multiphasic electrocardiogram (ECG) gated computed tomography (CT) by image registration and segmentation techniques.
Methods: Experimental validation was performed by evaluating a series of ECG gated CT scans of a stent graft moving at different amplitudes of displacement at different virtual heart rates using a motion generating device with synchronised ECG triggering. The methodology was further tested on clinical data of patients treated with EVAR devices with different stent graft designs. Displacement during the cardiac cycle was analysed for points on the fixating stent rings, the branches or fenestrations, and the spine.
Results: Errors for the amplitude of displacement measured in vitro at individual points on the wire frame were at most 0.3 mm. In situ cardiac induced displacement of the devices was found to differ per location and also depended on the type of stent graft. Displacement during the cardiac cycle was greatest in a fenestrated device and smallest in a chimney graft sac anchoring endosystem, with maximum displacement varying from 0.0 to 1.4 mm. There was no substantial displacement measurable in the spine.
Conclusions: A novel methodology to quantify and visualise stent graft motion in multiphasic ECG gated CT has been validated in vitro and tested in vivo. This methodology enables further exploration of in situ motion of different stent grafts and branch stents and their interaction with native vessels.

Keywords: Stent graft motion, Endovascular aneurysm repair, In vitro validation, Image registration, Dynamic quantification, ECG gated computed tomography
Article history: Received 10 December 2018, Accepted 7 March 2019, Available online 20 September 2019

* Corresponding author. Multi-modality Medical Imaging (M3I) group, Faculty of Science and Technology, Technical Medical Centre, University of Twente, PO Box 217, Enschede, 7500 AE, the Netherlands
E-mail address: m.a.koenrades@utwente.nl (Maaike A. Koenrades).

https://doi.org/10.1016/j.ejvs.2019.03.009

INTRODUCTION

Stent grafts are implanted in a dynamic endovascular environment, which undoubtedly affects long term patient outcome.[1,2] The long term outcome of endovascular aneurysm repair (EVAR) remains a reason for concern,[3—5] even though EVAR has become widely accepted for the

treatment of aortic aneurysms. The fixation and sealing of the stent graft to the aortic wall, is challenged with every heartbeat. If the sealing fails, blood flow can again enter the aneurysm sac resulting in type I endoleak, and the risk of rupture returns. Additionally, device configurations are becoming increasingly complex, including the use of fenestrated (FEVAR) and branched stent grafts (BEVAR), sac anchoring endosystems (EVAS), and chimney grafts (CHEVAR/CHEVAS),[6] which may jeopardise durability. Cardiac induced motions may cause component dislocation or detachment of the stent graft from the vessel wall, leading to migration, endoleak and/or kinking.[1,2] The forces on the stent may even change over time because of changes in stent expansion in patients presenting with neck dilatation. Stent graft migration and endoleak have been shown to be responsible for re-intervention within six years after endovascular treatment in 5—29% of patients.[6—9] Also, stent fracture may occur as a result of continuous cyclical deformation that exerts mechanical stress on the wire frame, resulting in fatigue. Depending on the type of stent graft and the location of the fracture, this may have serious consequences.[10,11] Conversion to resolve failing EVAR is accompanied by a substantial morbidity and mortality[12] and FEVAR in a failed EVAR device is complex and may lead to technical failure because of the inability to cannulate the side branches.[13]

Failure of EVAR may occur years after treatment. Besides anatomical changes over time, including neck enlargement, stent related factors could contribute to these late failures. Manufacturers use computational modelling and accelerated fatigue tests to optimise their designs. However, these techniques are mainly based on assumptions and often lack actual knowledge of in situ cardiac induced motion. A realistic simulation of the endovascular environment, including patient specific physiological and mechanical properties, is essential for accurate failure prediction.[1] Fatigue tests for example rely on the extent of stress and strain imposed on the wire frame of the stent graft. The reliability of computational techniques that aim to provide insight into the distribution of stress and strain, such as finite element analysis, depends greatly on the degree to which they can be validated against actual in situ measurements of strain. It is therefore highly relevant to obtain information on the motion of stent grafts in situ, both to perform risk assessment in the preclinical stage during device development and for early prediction of failure in the individual patient in post-market evaluations of new or modified devices.

Detailed knowledge on the motions of implanted stent grafts is limited, since routine follow up imaging is commonly restricted to static computed tomography (CT) that does not allow for measurement of motion. Electrocardiogram (ECG) gated (3D + time) CT can be used to quantify motions of stent grafts[14,15] and the aortic vessel,[2,16—23] although validation studies are scarce.[24,25] Most studies have evaluated pulsatile distension of the aorta during the cardiac cycle by measuring aortic dimensions perpendicular to a central luminal line in multiplanar reconstructions at predetermined levels.[2,17—23] A disadvantage of using two dimensional cross sectional images is that it does not allow for correction of movement out of plane in a cranial or caudal direction and thus does not allow for three dimensional measurement of motion. Also, in these studies measurements were performed separately in each of the reconstructed phases, which is prone to measurement inaccuracies, resulting in relatively high observer variability in the range of the measured motion.[19,20] Moreover, there was no reference for the actual in situ motion to validate the measurements.

The current study was conducted to provide accurate data characterizing the motion of implanted stent grafts. The method used was based on a previously established combination of an image registration and a segmentation algorithm to quantitatively and qualitatively assess motions of stent grafts and their interaction with native vessels in time resolved CT data.[15] The method was validated in vitro and further tested on clinical data of patients treated by EVAR devices with different stent graft designs.

METHODS

In vitro validation experiments

Experimental set up. A motion generating device with synchronised ECG triggering (PC controlled phantom device, QRM Quality Assurance in Radiology and Medicine GmbH, Möhrendorf, Germany[26]) was used to obtain a series of ECG gated CT scans with a stent graft moving according to predetermined patterns with different amplitudes of motion at different virtual heart rates. The main body of an Anaconda stent graft (Terumo Aortic, Inchinnan, UK) was attached to the lever of the motion device. The body of this stent graft comprises two nitinol O-shaped stent rings to provide fixation and sealing of the stent graft against the vessel wall. The lever was placed in a water filled polyacrylic container with cylindrical tube (diameter, 45 mm; wall thickness, 2 mm) to fit the hole of an anthropomorphic aortic abdomen phantom (QRM GmbH; dimensions *xyz*, 300 × 200 × 250 mm^3; lumen diameter, 45 mm). This phantom was developed to mimic a cross section of the human abdomen for CT imaging, comprising spine, kidneys, and soft tissue equivalent material. The experimental set up is shown in Fig. 1.

Abdominal aortic motion patterns. A motion pattern composed of Gaussian functions was designed to mimic aortic motion. By providing the pattern's frequency and amplitude, two series of motion patterns were generated. In the A series the heart rate was changed while the amplitude remained constant, and vice versa in the B series. Note that with amplitude the maximum absolute value of displacement is referred to, that is the maximum distance between two positions during a full cycle. Two motion patterns in the B series were given a second peak to simulate irregular aortic motion, resembling non-uniform patterns[27] and wave reflection patterns.[28] The

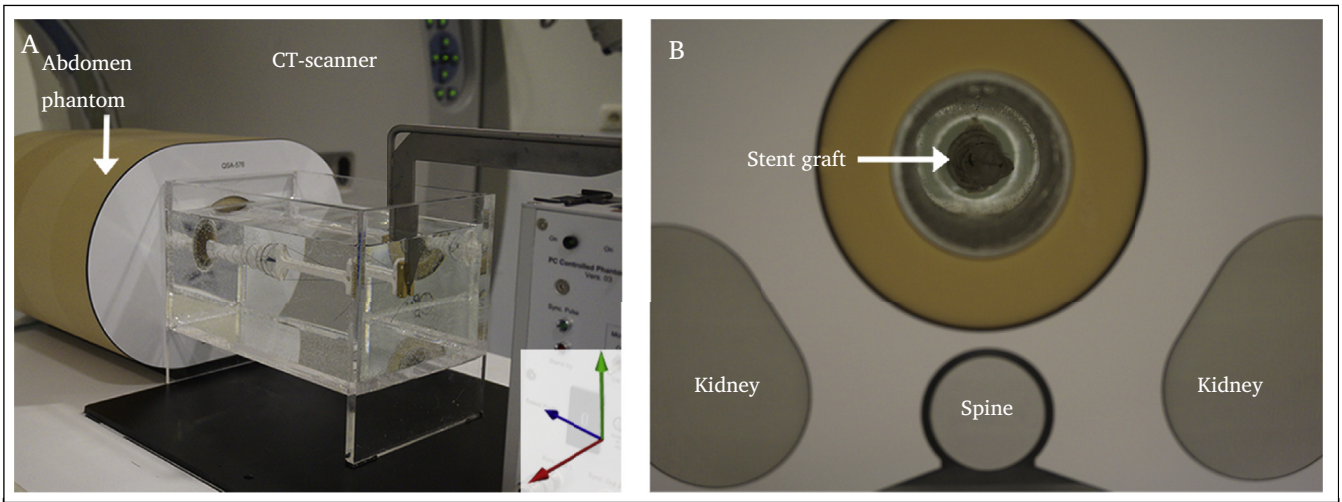

Figure 1. The experimental set up with CT scanner: the stent graft was moving in z direction (A) inside the aortic abdomen phantom (B). The axes of the coordinate system (A) denote the x (red), y (green), and z direction (blue). CT = computed tomography.

amplitudes chosen were relatively small since the stent graft is expected to locally decrease the motion of the abdominal aorta, which has been reported to be in the order of 1—2 mm.[16,27] Detailed information on the generated motion patterns is available in Supplementary material 1.

Validation of the motion device. To obtain a sub-millimetre accurate ground truth for algorithm validation, a high resolution camera was used to assess the patterns executed by the motion device. Details of this in vitro validation and the acquired reference patterns are available in Supplementary material 1 and corresponding Video S1 and S2.

ECG gated CT scans. Experiments were performed on two CT scanners that were recently used to acquire ECG gated CT scans in a clinical trial (Trialregister.nl identifier NTR4276): an Aquilion 64 CT scanner (Toshiba Medical Systems Corporation, Tokyo, Japan) and a Somatom Definition Flash CT scanner (Siemens Healthineers, Forchheim, Germany). The motion device was scanned with a helical scan protocol while executing the generated motion patterns. Time resolved ECG gated scans were obtained by triggering the CT scanners with the motion device. Scan and reconstruction parameters were in accordance with the clinical trial and were similar for both scanners: rotation time, 0.4 seconds (Aquilion), 0.285 seconds (Flash); collimation, 64 × 0.5 mm (Aquilion), 2 × 128 × 0.6 mm (Flash); slice thickness, 1 mm; slice overlap (increment), 0.5 mm; tube voltage, 120 kV; tube current time product, 60 mAs. Data were reconstructed with a FC12 (Aquilion) and I36f (Flash) convolution kernel, a matrix size of 512 × 512 pixels, and a field of view of approximately 250 × 250 mm^2, resulting in approximately isotropic voxels of 0.5 mm^3. The pitch factor was set automatically, based on the heart rate by which the duration of the scans varied between 10 and 20 seconds. Retrospective gating was applied to obtain 10 equidistant volumes covering the cardiac cycle (i.e., 0—90% of the RR interval). The resulting data were cropped to 256 × 256 × 200 voxels (*xyz*) to reduce memory requirements.

Motion modelling by image registration and segmentation. Motion of the stent graft was quantitatively and qualitatively assessed by applying a combined image registration and segmentation algorithm.[15,29,30] This method involved three steps: (1) deformable (i.e., elastic) registration of the time resolved 3D volumes to acquire deformation (i.e., vector) fields that describe the displacement of all voxels in all phases with respect to the average of all phases (hereafter referred to as time averaged volume); (2) segmentation of the stent rings, resulting in a geometric model that represents the wire frame and consists of nodes at wire crossings and edges connecting the nodes; and (3) applying the deformation fields to the geometric model to assess motion of the model throughout the phases. This process is illustrated in Fig. 2. Detailed information is provided in Supplementary material 2. The algorithms were coded in Python programming language (version 3).

Algorithm validation. Displacement patterns of the models as estimated by the algorithm were compared with the motion device reference patterns. The node points (8 per ring) and the points halfway along the edges of the rings (8 per ring) were used, resulting in 32 points per model. Errors were calculated by subtracting the values of maximum displacement, that is, pattern amplitudes errors, and by subtracting the respective patterns over the full cardiac cycle by taking the reference pattern positions at the correct times, that is, the positions at 10 equidistant time intervals corresponding to the 10 volumetric phases of the gated CT scans.

Statistics. Data were normally distributed and summarised as mean ± standard deviation and range, and were compared between the two CT scanners using a dependent Student's *t*-test for paired samples. A p values < .05 was

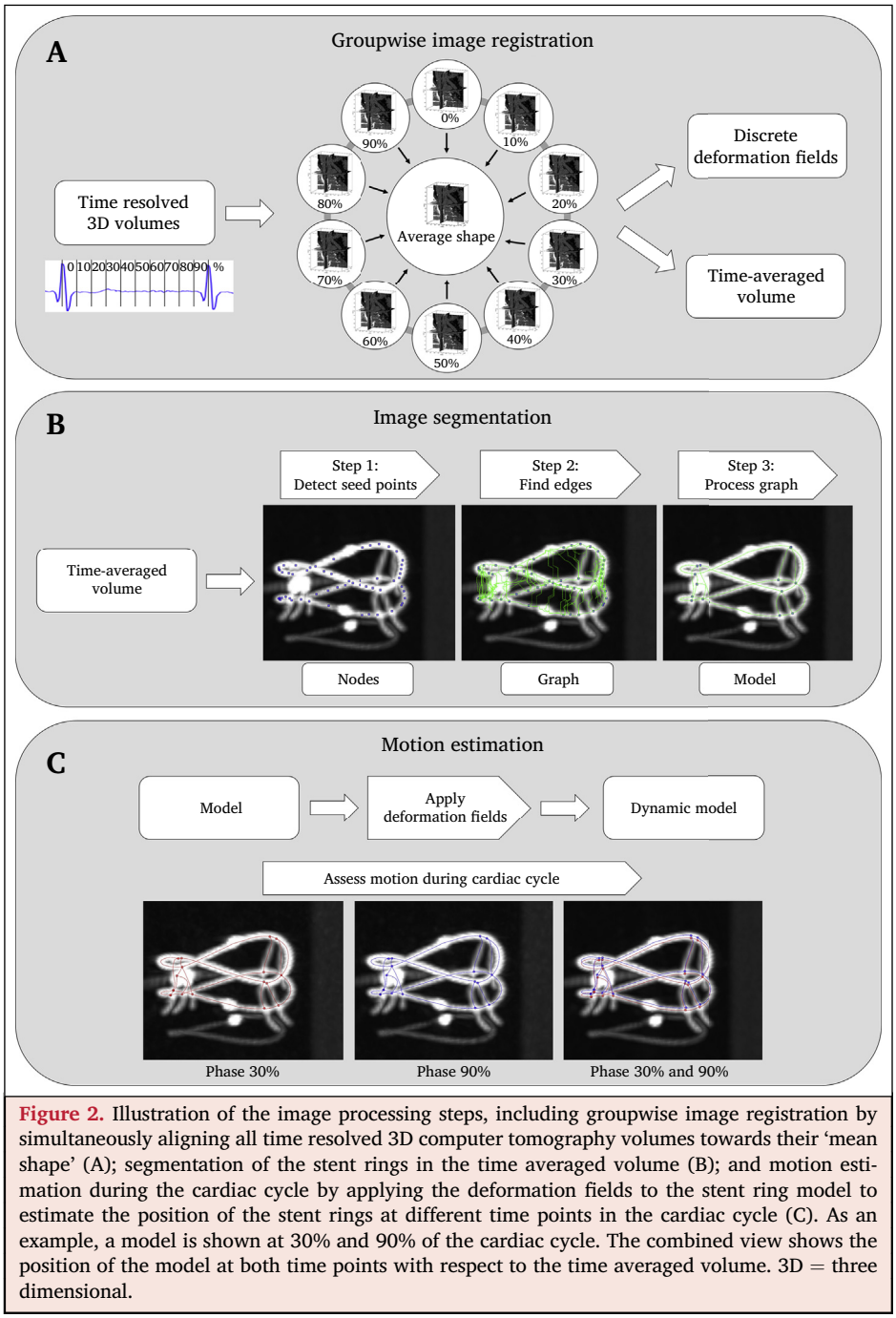

Figure 2. Illustration of the image processing steps, including groupwise image registration by simultaneously aligning all time resolved 3D computer tomography volumes towards their 'mean shape' (A); segmentation of the stent rings in the time averaged volume (B); and motion estimation during the cardiac cycle by applying the deformation fields to the stent ring model to estimate the position of the stent rings at different time points in the cardiac cycle (C). As an example, a model is shown at 30% and 90% of the cardiac cycle. The combined view shows the position of the model at both time points with respect to the time averaged volume. 3D = three dimensional.

considered significant. Statistical analysis was performed using the open source statistical functions of Scipy 1.1 with Miniconda3 as Python interpreter (Python 3).

Clinical application. The clinical applicability of the algorithm was evaluated using post-operative ECG gated CT scans of two EVAR cases (Anaconda device, Terumo Aortic, Inchinnan, Scotland, UK; Endurant device, Medtronic, Santa Rosa, CA, USA), a FEVAR case (Fenestrated Anaconda device, Terumo Aortic) employing Advanta V12 covered stents (Maquet Getinge Group, Hudson, NH, USA), and a CHEVAS case (Nellix device, Endologix, Irvine, CA, USA) also employing Advanta V12 covered stents. The EVAR and FEVAR data were collected from clinical trial databases (Trialregister.nl identifier NTR4276 and NTR6225, respectively). The CHEVAS case was retrospectively retrieved from the ASCEND registry.[31] The data collection was approved by local ethics committees. The ECG gated CT scans comprised 10 time resolved CT volumes at 10% steps of the cardiac cycle. Three dimensional displacement patterns were assessed for distinctive points on the proximal stent rings and the branches or fenestrations by applying the image registration and segmentation algorithm. For validation purposes, the displacement of points in the spine was assessed.

RESULTS

In vitro validation

The groupwise registration process took approximately 12 minutes per scan on an Intel Core i7-5500U processor with 2.9 GHz clock speed and 16 GB RAM. An example of a scan and obtained dynamic stent ring model is shown in Fig. 3. Fig. 4 compares reference patterns with algorithm patterns for the CT data that was obtained on each scanner. Table 1 presents the absolute values of the amplitude errors. Mean amplitude errors were smaller than 0.11 mm and 0.21 mm for the image data acquired on the Aquilion and Flash scanner respectively. The maximum amplitude error for a single point in the model was 0.27 mm (B4) for the Aquilion data and 0.30 mm (B6) for the Flash data. Small but statistically significant differences were noted between amplitude errors for the Aquilion and Flash data for the patterns A1 ($p = .045$), A3 ($p = .040$), B0 ($p = .001$), B1 ($p = .001$), B2 ($p = .004$), and B3 ($p = .003$). Absolute errors over the full cycle (all 10 positions/phases) are presented in Fig. 5. The difference between errors for the Aquilion and Flash data was small but statistically significant for the patterns A1 ($p < .001$), A2 ($p = .040$), B0 ($p < .001$), B1 ($p < .001$), B2 ($p < .001$), B4 ($p = .006$), and B6 ($p = .020$). Overall, mean absolute errors were smaller than 0.14 mm and 0.12 mm for the Aquilion and Flash data respectively.

Supplementary video related to this article can be found at https://doi.org/10.1016/j.ejvs.2019.03.009.

Clinical application

Fig. 6 presents cardiac induced displacement patterns in clinical ECG gated CT data of an Anaconda (Fig. 6A), an Endurant (Fig. 6B), a Fenestrated Anaconda (Fig. 6C), and a Chimney Nellix (Fig. 6D) configuration. The amplitude of displacement over the cardiac cycle was greatest in the fenestrated case and smallest in the Nellix case, varying from 0.0 to 1.4 mm. As was expected, the peaks in the stent graft motion patterns were found during the systolic phases

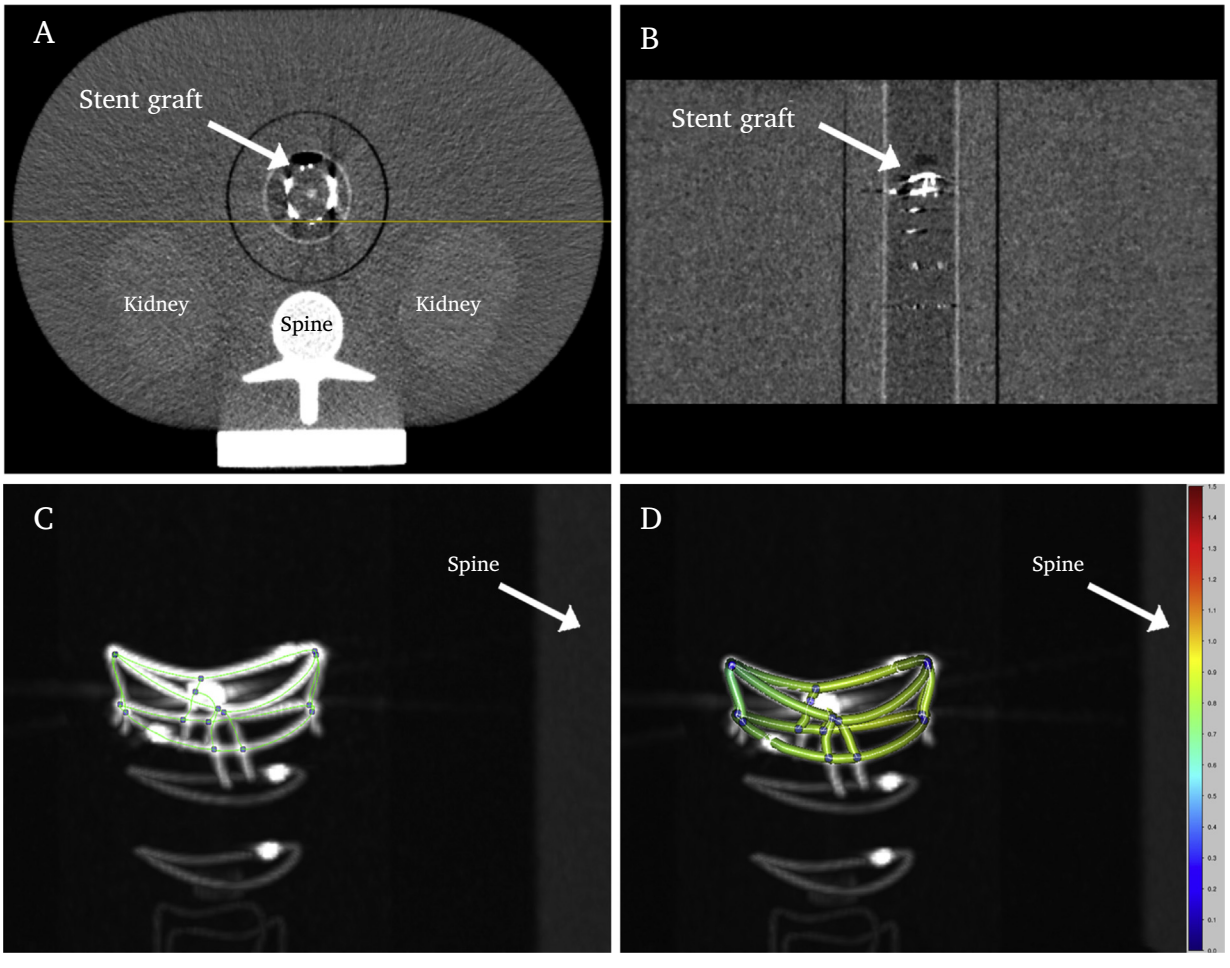

Figure 3. Example of a dynamic model that was acquired from the Aquilion CT (computed tomography) data (motion pattern A3), showing an axial (A) and coronal (B) multiplanar reconstruction (MPR) slice of the time averaged volume and three dimensional maximum intensity projections with the geometric model of the two upper rings (C,D) for which the amplitude of motion is visualised in a color coded mesh on a scale from 0 to 1.5 mm (D, Video S3). The yellow horizontal line in the axial MPR slice (A) indicates the level of the coronal slice (B). The green lines and blue dots (C,D) represent the model edges and node points, respectively.

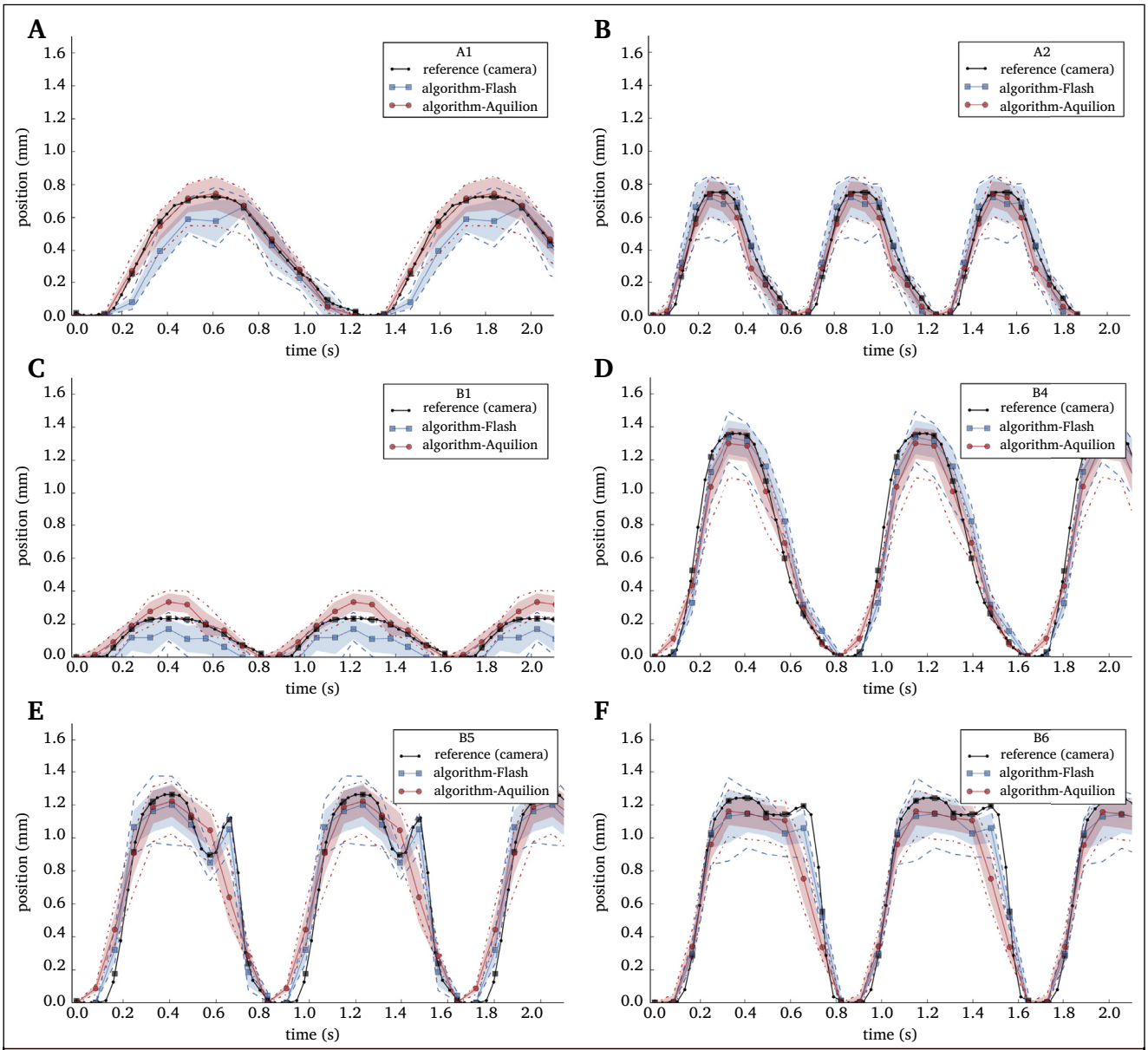

Figure 4. Reference vs. algorithm for both the Aquilion and the Flash computed tomography scanner for six motion patterns (A–F). Mean ± standard deviation of the algorithm patterns is shown as well as the patterns showing the minimum and maximum displacement (dashed/dotted lines). The black squares in the reference patterns correspond to each of the 10 reconstructed phases in the cardiac cycle to compare algorithm and reference.

of the cardiac cycle for the abdominal aorta. In all cases, the amplitude of displacement of the stent graft was above the uttermost error threshold of 0.3 mm, except for the Nellix case where only the branch showed moderate displacement. There was no substantial displacement measurable in the spine (*x* direction, 0.19 ± 0.08 mm; *y* direction, 0.19 ± 0.10; *z* direction, 0.18 ± 0.08).

DISCUSSION

This study validates a novel methodology combining image registration and segmentation techniques to quantify stent graft motions on multiphasic ECG gated CT. Since an absolute ground truth is lacking in clinical data, a physical phantom was used to evaluate the accuracy of the methodology. This in vitro validation demonstrated that the error for the amplitude of motion at individual points on the stent rings was small and at most 0.3 mm, which is about half the pertinent voxel size. The clinical applicability of the algorithm was demonstrated for four different stent graft designs in EVAR, FEVAR, and CHEVAS cases. Because aortic wall compliance generally increases from the abdominal to the thoracic region,[32] it may be expected that the motion of the fixating stent rings differs per location. This was indeed observed in this study, where the relative displacement, caused by the cardiac cycle, varied between 0.0 and 0.7 mm. The maximum displacement also depended on the type of stent graft. It is also not surprising that there was virtually no movement of the Nellix device, which uses rigid polymer filled endobags to fill the aneurysmal lumen

Table 1. Experimental results of the pattern amplitude errors obtained for two CT scanners

P	A (mm)	Aquilion 64 CT scanner		Somatom Definition Flash CT scanner	
		Error (mm)	Error (%)	Error (mm)	Error (%)
A1	0.72	0.08 ± 0.05 (0.03–0.17)	12 ± 6 (4–24)	0.06 ± 0.05 (0–0.13)	8 ± 6 (0–18)
A2	0.75	0.07 ± 0.04 (0–0.15)	9 ± 6 (1–20)	0.09 ± 0.08 (0.02–0.24)	12 ± 10 (3–32)
A3	0.70	0.11 ± 0.05 (0.03–0.16)	16 ± 7 (5–23)	0.16 ± 0.06 (0.07–0.25)	23 ± 9 (9–36)
B0	0	0.03 ± 0.03 (0–0.08)	–	0.21 ± 0.03 (0.17–0.26)	–
B1	0.23	0.10 ± 0.05 (0.01–0.17)	43 ± 23 (6–73)	0.06 ± 0.04 (0.01–0.14)	27 ± 19 (5–58)
B2	0.37	0.06 ± 0.04 (0.02–0.12)	15 ± 10 (5–32)	0.16 ± 0.04 (0.09–0.21)	42 ± 10 (25–56)
B3	0.70	0.06 ± 0.03 (0–0.10)	8 ± 5 (2–15)	0.11 ± 0.08 (0.01–0.23)	16 ± 11 (1–32)
B4	1.38	0.06 ± 0.09 (0–0.27)	5 ± 7 (0–20)	0.07 ± 0.06 (0–0.16)	5 ± 4 (0–12)
B5	1.26	0.07 ± 0.07 (0–0.24)	6 ± 6 (0–19)	0.10 ± 0.09 (0.03–0.29)	8 ± 7 (2–23)
B6	1.24	0.09 ± 0.08 (0–0.23)	7 ± 6 (1–19)	0.13 ± 0.09 (0.01–0.30)	10 ± 7 (1–24)

Data are presented as mean ± standard deviation (range). Values are given in millimeters and as a percentage of A. A3 and B3 are repeated measures and have the same reference. CT = computed tomography; P = motion pattern; A = amplitude of reference pattern

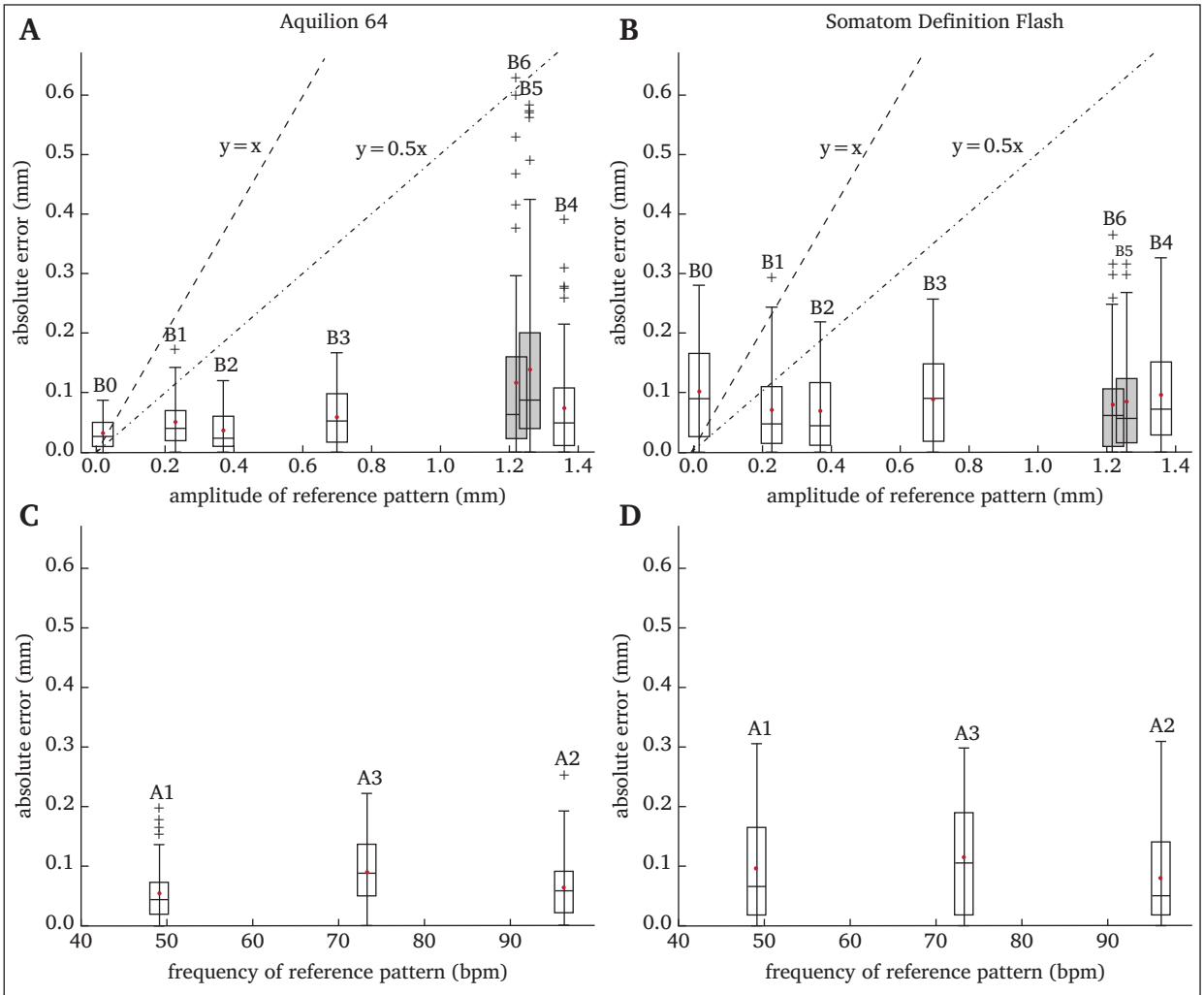

Figure 5. Absolute errors of the reference vs. the algorithm over the full cycle for all 10 positions (10 phases) in the displacement patterns (please refer to Fig. 4). Errors are shown for both the Aquilion (A,C) and the Flash (B,D) CT (computed tomography) image data for the patterns with varying amplitude (A,B) and frequency (C,D). The red dots represent mean absolute errors. The whiskers represent 1.5 times the interquartile range. The two patterns with an extra peak (B5, B6) are shown with gray boxes. Reference lines at $y=x$ and $y=0.5x$ are shown (A,B) to relate the error to the amplitude of motion. A3 and B3 are repeated measures and have the same reference. bpm = beats per minute.

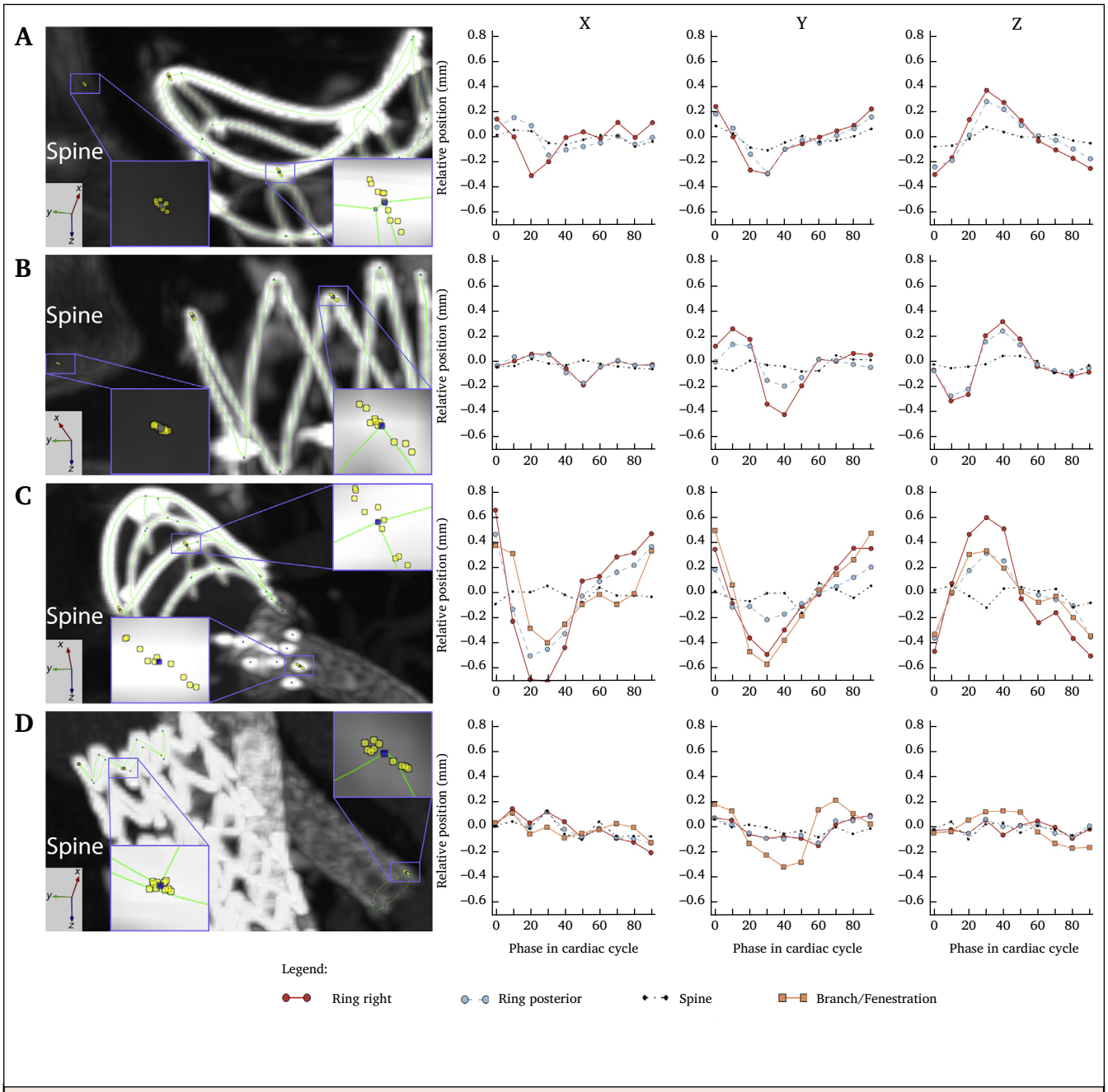

Figure 6. An in situ analysis of displacement during the cardiac cycle in post-operative ECG (electrocardiogram) gated CT (computed tomography) data of four abdominal aortic aneurysm patients who were treated endovascularly using an Anaconda (A), an Endurant (B), a Fenestrated Anaconda (C), or a Chimney Nellix (D) device configuration. Displacement is shown for individual points of the proximal stent rings, the fenestration or branch, and the spine. The three dimensional images display the position of the geometric models (model lines and blue dots) at mid–cardiac cycle in the time averaged volume and the position of distinct, individual points at each phase in the cardiac cycle (yellow dots) with higher magnifications in the boxes. For each case the graphs display the relative position of the individual points with respect to the time averaged volume as a function of the cardiac phase (in percent of RR interval) in *x*, *y*, and *z* direction, corresponding to the right (−) to left (+), anterior (−) to posterior (+), and cranial (−) to caudal (+) direction. The axes of the coordinate systems denote the *x* (red), *y* (green), and *z* direction (blue). RR interval = heart rate.

and stabilise two balloon expandable covered stents in the aorta and iliac arteries. Yet, the dynamic behaviour may change over time and can potentially be an early indicator of failure. More knowledge and understanding of this new endovascular treatment technique seems requisite, since the longer term outcomes appear to be significantly inferior to other available treatment options.[5]

While several studies have investigated the dynamic behaviour of the aorta,[2,16–23] including a recent study that employed deformable registration techniques for the aortic arch,[33] little has been reported on the dynamic behaviour of stent grafts. From a clinical point of view however, this information is of the utmost importance. Late failures after EVAR are not uncommon and necessitate prolonged follow

up. Early identification of those at risk of failure, may lead to a more individualised follow up scheme and reduce the burden of prolonged follow up. Langs et al.[14] have proposed a method to study motion of stent grafts in the thoracic aorta by applying a statistical shape variation model that is built during registration from a finite set of interest points, that is, landmarks on the wire frame. Using in situ patient data they evaluated correspondence quality of the registration by computing distances between original interest points in an individual phase of the cardiac cycle and interest points that were mapped according to the deformation field. They found mean registration errors between 0.25 and 0.73 voxels (in plane *xy* dimensions, 0.65 × 0.65 mm^2 to 0.98 × 0.98 mm^2; slice thickness, 0.625 mm) but did not report the errors of individual interest points. These registration errors appear to be higher than the errors reported in the present work, which may be explained by the fact that the statistical models are based on a set of landmarks rather than a texture based deformation of the entire volume as applied by the present algorithm.

In the in vitro validation experiments the results of two CT scanners were compared. Several patterns showed small yet statistically significant differences between the scanners. Several factors may have contributed to such differences, including the hardware of the scanners, the reconstruction process (e.g., interpolation, filtering), and the temporal resolution (Aquilion 200 ms vs. Flash 75 ms). Notably, the extra peaks that were added in two patterns were not identified in the data of the Aquilion scanner, but these were identified in the data of the Flash scanner (Fig. 4E and F). Overall, there was no consistent under or overestimation of motions when comparing the errors of both scanners, which suggests that results would not require correction when comparing clinical data from the respective scanners.

A limitation of this work is that the experimental validation was performed in *z* direction only. Nevertheless, three dimensional displacement patterns were analysed in clinical ECG gated CT data, demonstrating that pulsatile motions can be measured in all three directions and may differ between stent grafts. Additionally, there was no substantial motion in the spine, which suggests that the measured in vivo stent graft motion was cardiac induced and not due to image artefacts or registration errors. Moreover, it was expected that the performance in *x* and *y* direction is equal to or even better than the performance in *z* direction since, although the voxel dimensions were approximately the same in all dimensions (0.5 mm), the effective spatial resolution was higher in the *x*—*y* dimensions because the slice thickness was 1 mm. Also, in previous work it was found that the detectability of motions was better in *x* direction than in *z* direction.[25] Furthermore, even though pulsatile displacement profiles were mimicked, the motion was simplified compared with the situation in vivo where the blood flow may also deform the stent graft and the aorta (e.g., radial expansion), which may be more difficult to measure. Nonetheless, the employed deformable registration allows measurement of such complex transformations.[30] Additional experiments may be performed with more realistic motion patterns by, for example, using synthetic data with known deformation fields or real world patient data with extracted landmark trajectories, since it is virtually not feasible to validate subtle deformations in physical experimental models.

This study provides evidence that the proposed algorithm is able to accurately measure (subvoxel) motions of aortic stent grafts in ECG gated CT. This enables measurement of subtle cardiac induced adaptations of the stent graft in the aortic neck and therewith to evaluate the consequences of stent grafting on aortic neck compliance. Moreover, such measurements allow for adequate preclinical tests and early clinical assessment of stent graft efficacy and durability, including risk assessment for endoleak, migration, stent dislocation, and/or fracture.

CONCLUSION

Using a motion generating device, this study has demonstrated that the accuracy of the proposed registration and segmentation technique is adequate for measurement of abdominal aortic stent graft motions on ECG gated CT data. Errors for the amplitude of motion at individual points on the stent rings were no more than 0.3 mm, which supports the feasibility of measuring subtle motions in vivo. The algorithm was successfully applied to clinical ECG gated CT data to measure and visualise three dimensional motions during the cardiac cycle in EVAR, FEVAR, and CHEVAS cases with different Z and O shaped stent graft designs. This novel methodology offers the prospect to investigate in situ behaviour of different stent grafts and branch stents in the dynamic endovascular environment of the thoracoabdominal aorta and branches.

ACKNOWLEDGMENTS

The authors thank the Department of Radiology of the Medisch Spectrum Twente and Bert Klein Rot (Chief laboratory technician CT) in particular for providing technical support with the CT acquisitions. Furthermore, the authors thank the Department of Radiology of the University Medical Centre Groningen (UMCG) and prof.dr. Marcel J.W. Greuter (Head of Medical Physics UMCG) for providing us their QRM motion device to test the setup. Finally, the authors thank prof.dr.ir. Bernard J. Geurts (Chairholder for Multiscale Modelling and Simulation in the Department of Applied Mathematics at the University of Twente) for critically reviewing the article.

CONFLICTS OF INTEREST

None.

FUNDING

The work was funded in part by an unrestricted research grant from Vascutek Terumo, trading as Terumo Aortic, and in part by the PPP Allowance made available by Health~Holland, Top Sector Life Sciences & Health, to stimulate public-private partnerships.

APPENDIX A. SUPPLEMENTARY DATA

Supplementary data related to this article can be found online at https://doi.org/10.1016/j.ejvs.2019.03.009.

REFERENCES

1 Chuter TAM. Durability of endovascular infrarenal aneurysm repair: when does late failure occur and why? *Semin Vasc Surg* 2009;**22**:102–10.
2 Van Keulen JW, Moll FL, Barwegen GK, Vonken EPA, Van Herwaarden JA. Pulsatile distension of the proximal aneurysm neck is larger in patients with stent graft migration. *Eur J Vasc Endovasc Surg* 2010;**40**:326–31.
3 Thomas B, Sanchez L. Proximal migration and endoleak: impact of endograft design and deployment techniques. *Semin Vasc Surg* 2009;**22**:201–6.
4 Ilyas S, Shaida N, Thakor AS, Winterbottom A, Cousins C. Endovascular aneurysm repair (EVAR) follow-up imaging: the assessment and treatment of common postoperative complications. *Clin Radiol* 2015;**70**:183–96.
5 Verhoeven ELG, Mani K. New technology failures: who to blame or time to be cautious? *Eur J Vasc Endovasc Surg* 2018;**56**:318–9.
6 Buck DB, van Herwaarden JA, Schermerhorn ML, Moll FL. Endovascular treatment of abdominal aortic aneurysms. *Nat Rev Cardiol* 2014;**11**:112–23.
7 Hobo R, Buth J. Secondary interventions following endovascular abdominal aortic aneurysm repair using current endografts. A EUROSTAR report. *J Vasc Surg* 2006;**43**:896–902.
8 Troisi N, Donas KP, Austermann M, Tessarek J, Umscheid T, Torsello G. Secondary procedures after aortic aneurysm repair with fenestrated and branched endografts. *J Endovasc Ther* 2011;**18**:146–53.
9 De Bruin JL, Baas AF, Buth J, Prinssen M, Verhoeven ELG, Cuypers PWM, et al. Long-term outcome of open or endovascular repair of abdominal aortic aneurysm. *N Engl J Med* 2010;**362**:1881–9.
10 Verhoeven ELG, Vourliotakis G, Bos WTGJ, Tielliu IFJ, Zeebregts CJ, Prins TR, et al. Fenestrated stent grafting for short-necked and juxtarenal abdominal aortic aneurysm: an 8-year single-centre experience. *Eur J Vasc Endovasc Surg* 2010;**39**:529–36.
11 Roos JE, Hellinger JC, Hallet R, Fleischmann D, Zarins CK, Rubin GD. Detection of endograft fractures with multidetector row computed tomography. *J Vasc Surg* 2005;**42**:1002–6.
12 Kansal V, Nagpal S, Jetty P. Editor's choice - late open surgical conversion after endovascular abdominal aortic aneurysm repair. *Eur J Vasc Endovasc Surg* 2018;**55**:163–9.
13 Falkensammer J, Taher F, Uhlmann M, Hirsch K, Strassegger J, Assadian A. Rescue of failed endovascular aortic aneurysm repair using the fenestrated Anaconda device. *J Vasc Surg* 2017;**66**:1334–9.
14 Langs G, Paragios N, Desgranges P, Rahmouni A, Kobeiter H. Learning deformation and structure simultaneously: in situ endograft deformation analysis. *Med Image Anal* 2011;**15**:12–21.
15 Klein A, Renema W, Vliet JA, Oostveen LJ, Hoogeveen Y, Schultze Kool LJ, et al. *Motion calculations on stent grafts in AAA. Diagnosis, screening and treatment of abdominal, thoracoabdominal and thoracic aortic aneurysms*. Rijeka: InTech; 2011. p. 125–44.
16 van Keulen JW, van Prehn J, Prokop M, Moll FL, van Herwaarden JA. Dynamics of the aorta before and after endovascular aneurysm repair: a systematic review. *Eur J Vasc Endovasc Surg* 2009;**38**:586–96.
17 Teutelink A, Muhs BE, Vincken KL, Bartels LW, Cornelissen SA, van Herwaarden JA, et al. Use of dynamic computed tomography to evaluate pre- and postoperative aortic changes in AAA patients undergoing endovascular aneurysm repair. *J Endovasc Ther* 2007;**14**:44–9.
18 Iezzi R, Di Stasi C, Dattesi R, Pirro F, Nestola M, Cina A, et al. Proximal aneurysmal neck: dynamic ECG-gated CT angiography—conformational pulsatile changes with possible consequences for endograft sizing. *Radiology* 2011;**260**:591–8.
19 van Keulen JW, Vincken KL, van Prehn J, Tolenaar JL, Bartels LW, Viergever MA, et al. The influence of different types of stent grafts on aneurysm neck dynamics after endovascular aneurysm repair. *Eur J Vasc Endovasc Surg* 2010;**39**:193–9.
20 Pol JA, Truijers M, van der Vliet JA, Fillinger MF, Marra SP, Renema WKJ, et al. Impact of dynamic computed tomographic angiography on endograft sizing for endovascular aneurysm repair. *J Endovasc Ther* 2009;**16**:546–51.
21 Muhs BE, Vincken KL, van Prehn J, Stone MKC, Bartels LW, Prokop M, et al. Dynamic cine-CT angiography for the evaluation of the thoracic aorta; insight in dynamic changes with implications for thoracic endograft treatment. *Eur J Vasc Endovasc Surg* 2006;**32**:532–6.
22 Ganten MK, Krautter U, Von Tengg-Kobligk H, Böckler D, Schumacher H, Stiller W, et al. Quantification of aortic distensibility in abdominal aortic aneurysm using ECG-gated multi-detector computed tomography. *Eur Radiol* 2008;**18**:966–73.
23 de Beaufort HWL, Nauta FJH, Conti M, Cellitti E, Trentin C, Faggiano E, et al. Extensibility and distensibility of the thoracic aorta in patients with aneurysm. *Eur J Vasc Endovasc Surg* 2017;**53**:199–205.
24 Ganten M, Boese JM, Leitermann D, Semmler W. Quantification of aortic elasticity: development and experimental validation of a method using computed tomography. *Eur Radiol* 2005;**15**:2506–12.
25 Klein A, Oostveen LJ, Greuter MJWW, Hoogeveen Y, Schultze Kool LJ, Slump CH, et al. Detectability of motions in AAA with ECG-gated CTA: a quantitative study. *Med Phys* 2009;**36**:4616–24.
26 QRM quality Assurance in Radiology and medicine GmbH. Motion simulator Sim2D. http://www.qrm.de/content/products/dynamic/sim2d.htm. 05/20/2015.
27 Flora HS, Woodhouse N, Robson S, Adiseshiah M. Micromovements at the aortic aneurysm neck measured during open surgery with close-range photogrammetry: implications for aortic endografts. *J Endovasc Ther* 2001;**8**:511–20.
28 Nichols WW. Clinical measurement of arterial stiffness obtained from noninvasive pressure waveforms. *Am J Hypertens* 2005;**18**:3–10.
29 Klein A, van der Vliet JA, Oostveen LJ, Hoogeveen Y, Schultze Kool LJ, Renema WKJ, et al. Automatic segmentation of the wire frame of stent grafts from CT data. *Med Image Anal* 2012;**16**:127–39.
30 Klein A, Kroon D-J, Hoogeveen Y, Schultze Kool LJ, Renema WKJ, Slump CH. Multimodal image registration by edge attraction and regularization using a B-spline grid. *Proc SPIE Med Imaging* 2011;**7962**:796220–8.
31 Thompson M, Youssef M, Jacob R, Zerwes S, Reijnen M, Szopinski P, et al. Early experience with endovascular aneurysm sealing in combination with parallel grafts for the treatment of complex abdominal aneurysms: the ASCEND registry. *J Endovasc Ther* 2017;**24**:764–72.
32 Schriefl AJ, Zeindlinger G, Pierce DM, Regitnig P, Holzapfel GA. Determination of the layer-specific distributed collagen fibre orientations in human thoracic and abdominal aortas and common iliac arteries. *J R Soc Interf* 2012;**9**:1275–86.
33 Nasr B, Le Ven F, Savean J, Ben Salem D, Nonent M, Gouny P, et al. Characterization of the physiological displacement of the aortic arch using non-rigid registration and MR imaging. *Eur J Vasc Endovasc Surg* 2017;**53**:282–9.